Pixelated RF: Random Metasurface Based Electromagnetic Filters

Jungmin Lee
MICS@VT
Virginia Tech
Blacksburg, VA
jmlee22@vt.edu

Wei Jia
ECE Dept.
University of Utah
Salt Lake City, UT, USA
happywei.jia@utah.edu

Berardi Sensale-Rodriguez
ECE Dept.
University of Utah
Salt Lake City, UT, USA
berardi.sensale@utah.edu

Jeffrey S. Walling
wireless@VT and MICS@VT
Virginia Tech
Blacksburg, VA, USA
jswalling@vt.edu

2023 21st IEEE Interregional NEWCAS Conference (NEWCAS) | 979-8-3503-0024-6/23/$31.00 ©2023 IEEE | DOI: 10.1109/NEWCAS57931.2023.10198065

***Abstract*—Recent trends in photonics have shown that optimized pixelated surfaces can outperform classical designs in reducing design area and improving frequency response. Such pixelated surfaces can also be used to realize random RF components (e.g., filters, matching networks, power splitters/combiners, etc.). There are no closed form solutions to describe the design of these surfaces. We present a method for synthesizing a pixelated surface to act as a filter using a direct binary search (DBS) to realize a dual-band RF filter. The method can be used to reliably create designs for generalizeable RF functions. To demonstrate the capability a prototype dual-band filter is fabricated on a printed circuit board (PCB) and occupies an area of $0.45 \times 0.34\text{in}^2$. The filter achieves a transmission loss of $< 2\text{dB}$ in the ISM band at 2.4 GHz and the UNII bands from $5.25-7.12\text{GHz}$, *using a low-cost 2-layer PCB and fabricated on a laboratory milling machine* without any complicated cross-sectional elements (e.g., cavity resonators, dielectric resonators, etc.).**

***Index Terms*—random RF components, pixelated RF, dual-band filter, microstrip, metasurface**

I. Introduction

With congested spectrum in the cellular communication and connectivity bands below 5GHz, filtering is increasingly important. A wireless receiver must be selective to a desired signal in the presence of interference that can be orders of magnitude larger. Passive filtering in wireless front-ends often consists of integrated LC filtering [1], or front-end modules using a single [2], or multiple acoustic-wave filters [3]. Such filters are preferred over electromagnetic filter structures (e.g., stepped-impedance, coupled-line, coupled resonator [4], etc.) because they provide higher out-of-band rejection in a more compact space and can often provide multiple passbands. Recently, it was demonstrated that pixelated planar conductive surfaces can be utilized to realize complex RF functions (e.g., wideband impedance matching, filtering and DC biasing [5]).

In a pixelated planar surface, a pixel is a uniform unit geometry of the top metal conductor that is tiled and can be populated with a conductor/metal or left unpopulated (e.g., exposed dielectric material), as shown in Fig. 1. Pixelated RF designs are difficult to realize because there are no closed-form methods for their design, and the design space is quite large ($\approx 2^N$, where N is the number of pixels). However, recent trends in photonics research have utilized various inverse-design methods for similar pixelated surfaces used at optical wavelengths, using optimization [6, 7] and machine learning methods [8–10]. Pixelated structures for photonics also have no closed form design solutions and as a result can look random and do not provide any intuition regarding their function or optimality, with designs seemingly constructed of arbitrarily placed pixels. Nevertheless, their performance has been demonstrated to be superior to classical design approaches for many common photonic structures [6, 11].

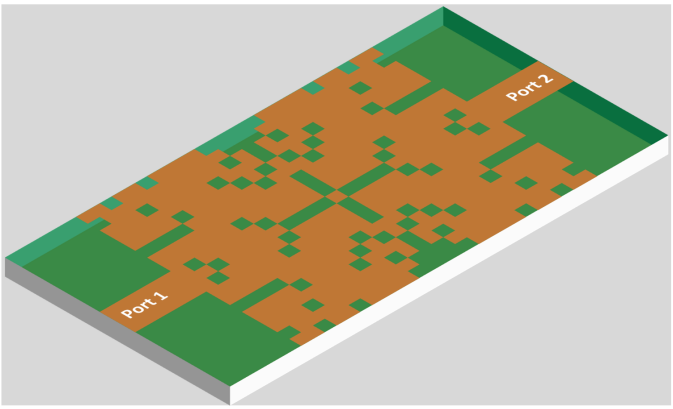

Fig. 1. Example of a pixelated RF planar surface.

Recently, artificial neural-networks (ANNs) have become resurgent with the use of "deep-learning". Deep-learning methods have become ubiquitous in inverse-design problems for photonic structures [12]. Using such methods, an ANN with multiple layers is trained to be a representative model of a complex structure. For instance, in the pixelated-RF domain, the ANN could be trained to model the frequency response (s-parameters) of any random set of pixels in a pixelated surface. Given enough training data, a model that is predictive of the frequency response would emerge that could be traversed in the reverse direction as well (e.g., given a specification of the frequency response, the model could be trained to provide a set of pixels that would optimally provide the desired response). Typically training data sets are built by randomly simulating pixelated surfaces using electromagnetic (EM) simulators and storing the pixel set and the corresponding frequency response. Tremendous amounts of data are typically required to make the inverse-design problem generalizable to any possible

frequency response. For instance for the 256 pixel design presented in [4], $>$ 70K data sets were required. Though it is phenomenal that designs can be realized with such a small fractional training set (e.g., $\approx 1/2^{240}$), still, each data set requires a few minutes for an EM simulation, meaning that several weeks to months can be required to acquire a sufficient training set.

Alternatively, search algorithms such as Direct Binary Search (DBS) can be employed [6]. In such searches, each pixel in a design is flipped during a single iteration and multiple iterations can be performed. After each pixel is flipped, an EM simulation is run and a Figure of Merit (FoM) is calculated. If improvement is detected in the FoM, the flipped pixel is kept; if the FoM is made worse, the change is discarded and a new pixel is flipped, and the process is repeated.

In this paper, a methodology for using DBS for the design of pixelated RF filters is described in section II. In section III, design details for a dual-band filter are provided. This is followed by measurement results in section IV for a laboratory fabricated filter that *demonstrates the potential to realize complex filters at very low cost and size*. Finally, conclusions and future work are presented in section V.

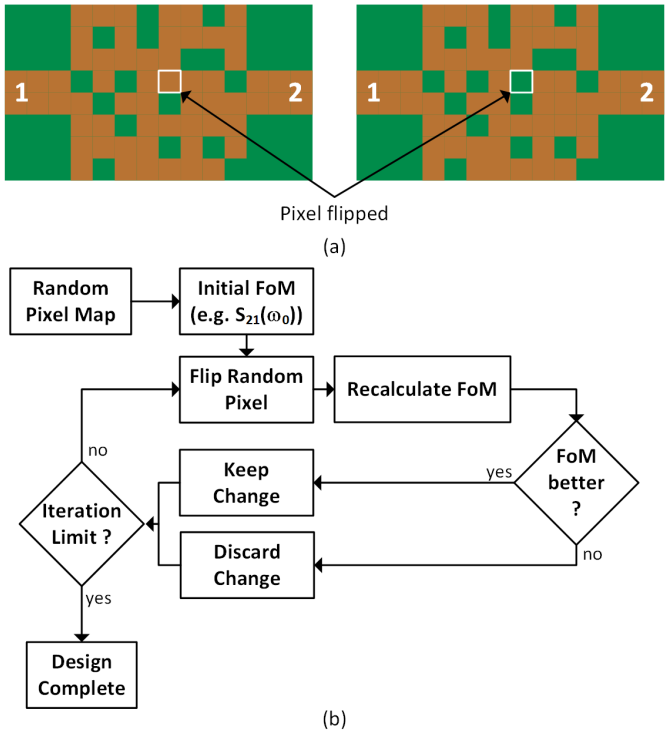

Fig. 2. (a) Random pixelated two-port microstrip circuit, demonstrating a pixel "flipping" operation. (b) DBS algorithm.

II. Pixelated RF Filter Design using Direct Binary Search

The proposed procedure for DBS-based filter design is illustrated in Fig. 2. A random surface is drawn as a graphics stream file in a "gdsii" format. The stream file contains artwork that depicts the random surface, as shown in Fig. 2(a). In the figure, a random two-port microstrip circuit is shown, and also a pixel "flip" is demonstrated in which an individual pixel is "flipped" from metal to dielectric.

In the basic procedure for DBS as shown in Fig. 2(b), a random pixelated surface is drawn. The circuit is simulated using an EM simulator to find its initial S-parameters and an optimization goal is specified as an FoM. In the illustration, the FoM is to increase the signal transmission (S_{21} at a frequency of ω_0. Next, a random pixel is flipped (e.g., from metal-to-dielectric or dielectric-to-metal) and a new EM simulation is run and the FoM is evaluated. If the FoM improved, the changed pixel is kept and a new pixel is flipped. If the FoM became worse, the changed-pixel is returned to its prior state and a new pixel is randomly chosen and flipped, with the remainder of the procedure repeating. In DBS, during an iteration, all pixels will be flipped once.

Convergence of a pixelated design using DBS is highly dependent on the initial starting point of the design [6], so it is common to allow the all of the pixels to flip multiple times in different iterations. Once the iteration limit is reached, the design process is complete. If the design is still not meeting specifications after the iteration limit, it can be used as the initial seed in a new round of DBS optimization, or another random seed can be tried. Though the process is iterative, it typically converges in a few hundred to a few thousand simulations, which is generally substantially fewer than are required to train an ANN.

To facilitate design, a toolbox has been created to generate random surfaces and run the DBS optimization. The toolbox is publicly available as a *github* repository [13], and is based upon a similar toolbox that was created for photonic design [14]. The toolbox allows generation of either random surfaces, or traditional microstrip designs (e.g., stepped impedance filters, tee-junctions, etc.) with up to four ports. It can control simulations in either *KeySight ADS* or *Cadence EMX*. The presented DBS method is slightly modified to allow for flipping of more than 1 pixel during each loop, which can be used with more iterations when the initial design is further away from achieving the optimization goals.

It is noted that all pixel operations are completed on a pixelmap array where the values are "1" for a pixel populated with metal and "0" for an unpopulated pixel. This allows easy boolean operations to define pixel flips and also relatively small storage requirements to save each pixelmap. The toolkit has functions to draw artwork files from the pixelmaps directly.

III. Dual-band Filter Design

In order to demonstrate the capabilities of the DBS method and the potential for pixelatedRF filters, we use the method to design a dual-band filter. A two-layer FR4 printed circuit board (PCB) is assumed, with the following physical parameters: $\epsilon_r = 4.5$, substrate thickness, $h = 62\text{mil}$, and metal thickness, $t = 1.4\text{mil}$. A pixel size of 18mil is used. To constrain the geometry, the area used by a third order stepped impedance

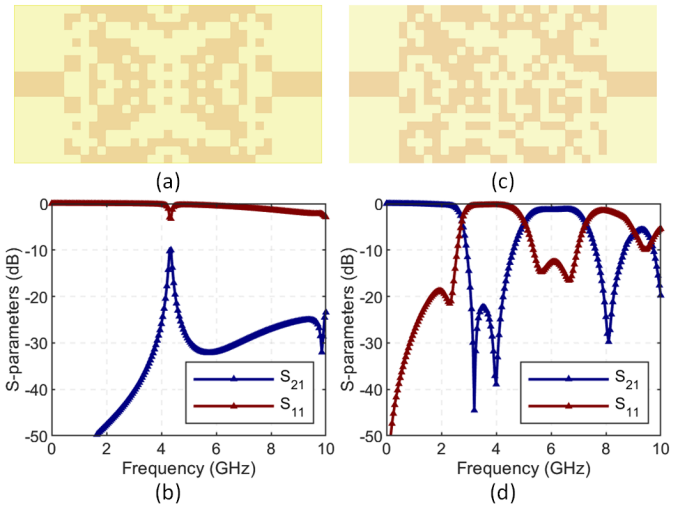

Fig. 3. (a) Initial random pixelatedRF surface. (b) Optimized pixelatedRF surface. (c) S-parameters of the initial design. (d) S-parameters of the optimized design.

filter sets the outer boundary of the filter, resulting in a pixelated surface consisting of 25×19 pixels (=475 pixels).

The dual-band filter is to be designed with a pass-band from DC-to-2.5GHz, a notch from 2.8-to-4.8GHz, and a passband from 5.5-to-7.5GHz. To define the optimization, seven primary goals are used. The first three goals are transmission requirements:

$$S_{21}(\omega)|_0^{2.5GHz} > -1\text{dB}, \tag{1}$$

$$S_{21}(\omega)|_{2.8GHz}^{4.8GHz} < -30\text{dB}, \text{and} \tag{2}$$

$$S_{21}(\omega)|_{5.5GHz}^{7.5GHz} > -1\text{dB}. \tag{3}$$

Additionally, the return loss requirements are specified:

$$S_{11}(\omega)|_0^{2.5GHz} < -10\text{dB}, \tag{4}$$

$$S_{11}(\omega)|_{5.5GHz}^{7.5GHz} < -10\text{dB}, \tag{5}$$

$$S_{22}(\omega)|_0^{2.5GHz} < -10\text{dB}, \text{and} \tag{6}$$

$$S_{22}(\omega)|_{5.5GHz}^{7.5GHz} < -10\text{dB}, \tag{7}$$

For each goal, the RMS error after the simulation is calculated and the errors for each goal are summed to create the FoM. The optimizer is written to minimize the FoM (e.g., drive the error towards zero).

In the presented case, the design starts with the random pixelated surface shown in Fig. 3(a). In the initial surface, each pixel is randomly assigned to either contain metal or not to contain metal. The S-parameters of the initial design are shown in Fig. 3(b). The random pixels, as expected, result in very low transmission and fail to meet the specifications. In the DBS optimization, 5 pixels ($\approx 1\%$) are allowed to flip on each trial. During each iteration, each pixel will be flipped exactly once. Since each trial consists of 5 pixels flipping, each iteration consists of $(475/5 = 95)$ trials. The trajectory of the FoM is plotted against the trial number in Fig. 4. In this example, after 210 trials, the FoM is < 0.03. The DBS simulation was allowed to run to its iteration limit (3 iterations = 285 trials), but no further reduction in the FoM was found after trial number 220. The final optimized design is shown in Fig. 3(c), with the corresponding S-parameters shown in Fig. 3(d). As can be seen from the S-parameter results, after optimization, the design achieves dual-band performance, with $< 3\% - \text{rms}$ error. Additional features that allow the optimization to climb out of local minima could result in a more optimal design. Additionally, allowing for smaller pixel size could result in more optimal designs.

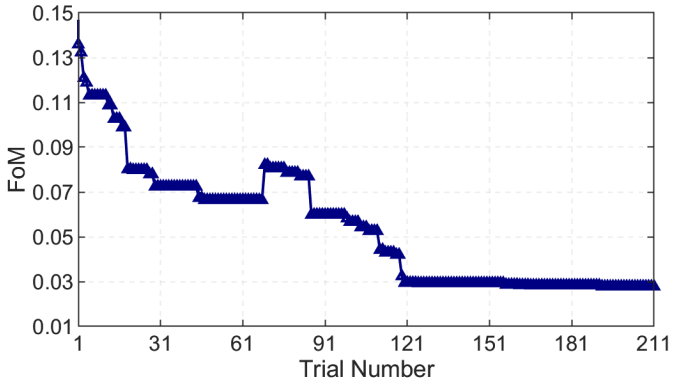

Fig. 4. Trajectory of the FoM during the optimization. Note the increase in the FoM at trial #70 was due to the optimization needing to be restarted in the middle of an iteration.

IV. Measurement Results

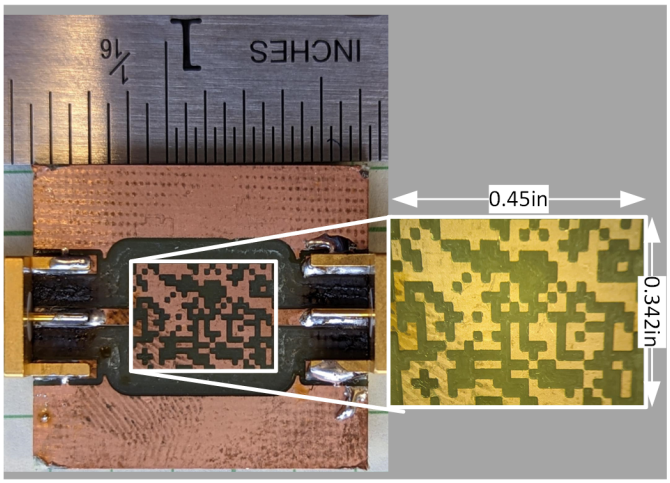

Fig. 5. Prototype pixelated RF filter design on a two-layer printed circuit board.

To demonstrate the potential of the pixelated design technique, a prototype pixelated dual-band RF filter is fabricated on a PCB (62mil thick FR4, $\epsilon_r = 4.5$, $tan\delta = 0.001$). It consists of 475 pixels arranged in a 25-$\times$-19 grid, as shown in Fig. 5. The filter is $\approx 0.45 \times 0.34$in, and with SMA connectors and routing added the PCB is $\approx 1 \times 1$in. The board

is fabricated using a CNC milling machine, which limited the minimum pixel size, based upon the finest milling tip that was available. This meant that diagonal connections between corner pixels could not be completely severed and hence the optimization was run considering that corner pixels would be physically connected, as can be seen in the inset of Fig. 5.

The S-parameters of the board are measured and compared to simulation results (including pads and interconnect) in Fig. 6. The measured input (S_{11}) and output (S_{22}) return loss are shown in Figs. 6(a) and (b), respectively. The measurements agree with the simulations quite well, with discrepancies primarily due to imperfect modelling of the SMA connector when using *Keysight Momentum*, which is a planar (2D) electromagnetic simulator. Additionally, the discrepancy at higher frequency is due to the FR4 material and would be expected to improve with dielectric materials optimized for higher frequency. *It is important to note that, though the filter does not achieve the same attenuation and roll-off as acoustic wave or cavity based filters, no complicated fabrication was used and this filter was fabricated with low-cost prototyping equipment that limited the pixel resolution*. It is expected that in the future, with more sophisticated printed fabrication on PCBs and ICs, or with higher quality materials, that filter responses similar to more expensive and lossier techniques can achieve. *Additionally, unlike acoustic filters, the principles that these filters work on are electromagnetic and hence it is expected that they can scale to higher frequency, provided technologies that allow the reduction in the pixel size, for instance those provided on integrated circuits.* The transmission (S_{21}) is measured in Fig. 6, and also agrees well with simulation. Discrepancies, particularly at higher frequency are primarily due to the dielectric material. The transmission loss is $< 2\text{dB}$ in the unlicensed bands at 2.4GHz and 5.25-7.125GHz and would be expected to improve with lower loss dielectric material and smaller pixel sizes.

V. Conclusions and Future Work

In this paper, pixelated RF surfaces are presented with the potential to realize RF passive networks including filters, power combiners/splitters, matching networks, diplexers, etc. There is no classical design methodology that can be followed to realize the filters; hence, an optimization method using direct-binary search is utilized. A representative filter is demonstrated on a printed circuit board, demonstrating a dual-band frequency response. The roll-off, attenuation and insertion loss of the presented filter is limited by the unit pixel size (e.g., 18mil) that was used in the design. It was chosen for ease of fabrication in rapid prototyping, but it is noted that in standard PCB fabrication, it is now possible to achieve pixel sizes $< 6\text{mil}$, even in low-cost fabrication. Furthermore, even smaller pixels can be realized in integrated circuit technologies. It is also noted that the designed structure consisted of a single layer of pixels, but future work may take advantage of multiple pixel layers that can be connected by vias to create more complicated frequency responses (e.g., more than 2-bands, deeper frequency notches, etc.).

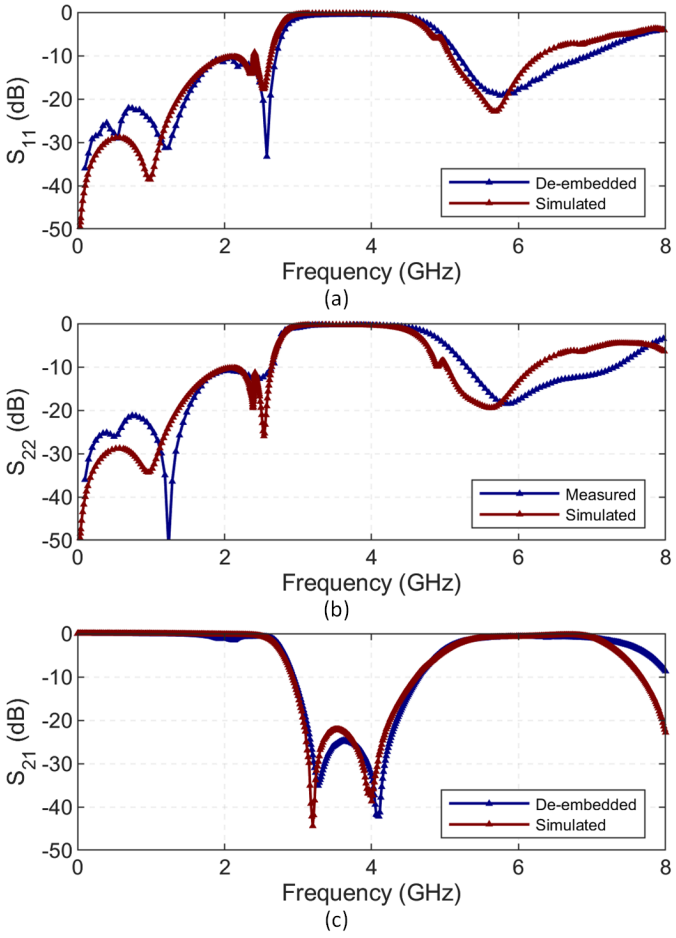

Fig. 6. Comparison of measured and simulated results for the prototype filter (a) S_{11}, (b)S_{22}, and (c) S_{21}.

References

[1] L. Mohammadi and K.-J. Koh, "A notch-feedback based 4th-order 2–4 GHz bandpass filter system for S-band radar receiver protection under the LTE and radar coexistence," in *2017 IEEE MTT-S International Microwave Symposium (IMS)*, 2017, pp. 1664–1667.

[2] Y. Shen, P. Patel, R. Vetury, and J. Shealy, "452 MHz bandwidth, high rejection 5.6 GHz UNII XBAW coexistence filters using doped AlN-on-silicon," in *2019 IEEE International Electron Devices Meeting (IEDM)*, 2019, pp. 17.6.1–17.6.4.

[3] D. Kim, J. I. Ryu, H.-M. Cho, N.-K. Kang, and J. C. Kim, "Implementation of a highly integrated triple-band RF front-end module," in *2007 Asia-Pacific Microwave Conference*, 2007, pp. 1–4.

[4] Y. Wu, K. Ma, and Y. Wang, "Design of in-line filter with cross-couplings paths and source loaded dangling resonator produced transmission zeros," in *2022 IEEE/MTT-S International Microwave Symposium - IMS 2022*, 2022, pp. 460–463.

[5] Z. Liu, E. A. Karahan, and K. Sengupta, "Deep learning-enabled inverse design of 30–94 GHz $P_{sat,3dB}$ SiGe PA supporting concurrent multiband operation at multi-Gb/s," *IEEE Microw. Wireless Compon. Lett.*, vol. 32, no. 6, pp. 724–727, 2022.

[6] B. Shen, P. Wang, R. Polson, and R. Menon, "An integrated-nanophotonics polarization beamsplitter with $2.4 \times 2.4\ \mu\text{m}^2$ footprint," *Nature Photonics*, vol. 9, no. 6, pp. 378–382, Jun. 2015, ISSN: 1749-4893. [Online]. Available: https://doi.org/10.1038/nphoton.2015.80.

[7] B. Ghaderi, V. Nayyeri, M. Soleimani, and O. M. Ramahi, "Pixelated metasurface for dual-band and multi-polarization electromagnetic energy harvesting," *Scientific Reports*, vol. 8, no. 1, p. 13 227, Sep. 2018,

ISSN: 2045-2322. [Online]. Available: https://doi.org/10.1038/s41598-018-31661-6.

[8] S. Molesky, Z. Lin, A. Y. Piggott, W. Jin, J. Vucković, and A. W. Rodriguez, "Inverse design in nanophotonics," *Nature Photonics*, vol. 12, no. 11, pp. 659–670, Nov. 2018, ISSN: 1749-4893. [Online]. Available: https://doi.org/10.1038/s41566-018-0246-9.

[9] S. Banerji, A. Majumder, A. Hamrick, R. Menon, and B. Sensale-Rodriguez, "Machine learning enables design of on-chip integrated silicon t-junctions with footprint of $1.2\mu\mathrm{m} \times 1.2\mu\mathrm{m}$," *Nano Communication Networks*, vol. 25, p. 100 312, 2020, ISSN: 1878-7789. [Online]. Available: https://www.sciencedirect.com/science/article/pii/S1878778920300818.

[10] S. Banerji, A. Majumder, A. Hamrick, R. Menon, and B. Sensale-Rodriguez, "Ultra-compact integrated photonic devices enabled by machine learning and digital metamaterials," *OSA Continuum*, vol. 4, no. 2, pp. 602–607, Feb. 2021. [Online]. Available: https://opg.optica.org/osac/abstract.cfm?URI=osac-4-2-602.

[11] A. Y. Piggott, J. Lu, K. G. Lagoudakis, J. Petykiewicz, T. M. Babinec, and J. Vučković, "Inverse design and demonstration of a compact and broadband on-chip wavelength demultiplexer," *Nature Photonics*, vol. 9, no. 6, pp. 374–377, Jun. 2015, ISSN: 1749-4893. [Online]. Available: https://doi.org/10.1038/nphoton.2015.69.

[12] W. Ma, Z. Liu, Z. A. Kudyshev, A. Boltasseva, W. Cai, and Y. Liu, "Deep learning for the design of photonic structures," *Nature Photonics*, vol. 15, no. 2, pp. 77–90, Feb. 2021, ISSN: 1749-4893. [Online]. Available: https://doi.org/10.1038/s41566-020-0685-y.

[13] J. S. Walling, *PixelatedRF*, 2022. [Online]. Available: https://github.com/noyades/pixelatedRF.

[14] Z. Zhao, *SPLayout*, 2022. [Online]. Available: https://github.com/Hideousmon/SPLayout.